BULLETIN OF THE EARTHQUAKE
RESEARCH INSTITUTE
Vol. 55 (1980), pp. 1-26

1. *Asymptotic Behavior of Spheroidal Eigenfrequencies of a Multi-Layered Spherical Earth.* — *Modes of Very High Phase Velocity* —

By Toshikazu ODAKA,

Earthquake Research Institute.

(Received Feb. 29, 1980)

Abstract

Derivation of a frequency equation is made in terms of the matrix formulation for spheroidal oscillations of a multi-layered spherical Earth. Then, it is shown that the equation splits at very high frequency into three independent equations corresponding to three body-wave types, *PKIKP*, $(ScS)_V$ and J respectively.

The result is used to obtain asymptotic frequency equations in explicit forms for simple Earth models consisting of a homogeneous liquid core and a one- to three-layered mantle. Comparison of those formulas leads to the conclusion that the equation for *PKP*-type and that for $(ScS)_V$-type are similar in form to each other when the number of internal discontinuities effective to respective body waves are the same. The fundamental difference in their forms is that the former equation depends on the evenness and oddness of the Legendre order while the latter one does not. It is proved through numerical computations that the solutions of the above equations to the first order approximation are useful for explaining asymptotic patterns of distribution of eigenfrequencies.

Further computations are made for two Earth models with realistic mantle structure, one with two distinct discontinuities in the upper mantle and the other with a continuously varying structure. Then, it is proved that in general there exists a remarkable difference between the two patterns of distribution of their eigenfrequencies. However the difference falls off at low frequencies because the whole upper-mantles, where elastic parameters change sharply with depth, act as the same scale of discontinuities on long-period free oscillations. Their patterns of oscillatory features are explainable in terms of an additive effect of the individual "solotone effect" associated with each discontinuity in the Earth.

1. Introduction

Since 1974, many investigations have been made on asymptotic behavior of eigenfrequencies of free oscillations of the Earth (*e.g.*,

ANDERSSEN and CLEARY, 1974; LAPWOOD, 1975; WANG *et al.*, 1977; SATO and LAPWOOD, 1977 a, b). These researches are mainly concerned with torsional oscillations and few papers refer to spheroidal oscillations (*e.g.*, ANDERSSEN *et al.*, 1975; GILBERT, 1975). There, especially, seems to be no quantitative discussion concerning spheroidal modes on the effect of discontinuities in the Earth on the distribution of the eigenfrequencies.

In this paper, we first derive a frequency equation for the spheroidal oscillations of a multi-layered spherical Earth in terms of the matrix method. Then, its asymptotic formula, valid at high frequency limit, is derived. Asymptotic frequency equations for simple Earth models are obtained in explicit forms and their solutions to the zero order and first order approximations are derived. Finally, numerical computation is made for two kinds of models, one with a very simple structure and the other with a rather realistic mantle structure, in order to confirm the validity of the above mentioned approximate solutions and to examine by experiments the effect of the discontinuities on the asymptotic patterns of the distribution of the eigenfrequencies.

The matrix method is equivalent to the so-called Thomson-Haskell method applied primarily to wave propagation in a plane stratified medium. Its principle is now familiar to us and we can find some applications to spherically stratified media (GILBERT and MACDONALD, 1960; BEN-MENAHEM, 1964b; PHINNEY and ALEXANDER, 1966; BHATTACHARYA, 1976). However, no expression of a spheroidal frequency equation for an Earth with a solid inner core seems to be directly available. Here, we will develop independent formulation to obtain the formal frequency equation in a form convenient for our present purpose. The effect of gravity is ignored since it is expected to be small for higher modes.

2. Frequency Equation for a Multi-Layered Earth

We assume that an Earth is formed of the crust/mantle, the liquid outer core and the solid inner core, each medium consisting of the stack of uniform spherical layers in welded contact. A realistic Earth model is obtained by increasing the number of uniform layers. The numbering of the layers and boundaries are shown in Fig. 1, where the numbers 1 through K refer to the inner core, $K+1$ through L to the outer core and $L+1$ through M to the mantle/crust respectively.

We denote radial factors of displacements and stresses for the spheroidal modes in a vector form as

$$\boldsymbol{y}_i(r)=(rU_i(r)\ ,\quad rV_i(r)\ ,\quad r^2S_i(r)\ ,\quad r^2T_i(r))^T\quad (r_{i-1}\leq r\leq r_i) \tag{2.1}$$

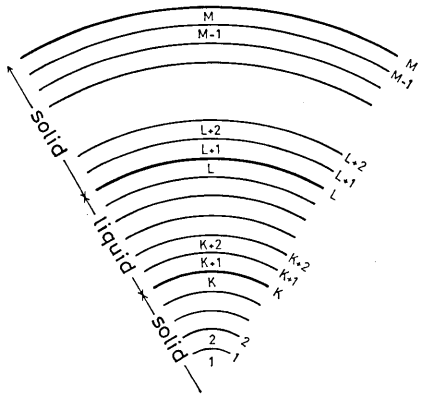

Fig. 1. Multi-layered Earth model consisting of the solid inner core (K layers), liquid outer core ($L-K$ layers) and mantle/crust ($M-L$ layers).

where U_i and V_i are the radial and tangential displacement components in the i-th layer, S_i and T_i the radial and tangential stress components acting on the plane normal to the radial direction. r means the radial distance and r_i that of the i-th interface. By the superscript T (transpose) we define $\boldsymbol{y}_i(r)$ as a column vector, which is, in a homogeneous and isotropic medium, given by

$$\boldsymbol{y}_i(r)=\boldsymbol{E}_i(r)\boldsymbol{c}_i \qquad (r_{i-1}\leq r\leq r_i)\ , \tag{2.2}$$

where

$$\begin{aligned}&\boldsymbol{E}_i(r)=(e^i_{jk}) \quad (j,\ k=1,\ 2,\ 3,\ 4)\ ,\\ &\boldsymbol{c}_i=(A_i,\ B_i,\ C_i,\ D_i)^T\ .\end{aligned} \tag{2.3}$$

$\boldsymbol{E}_i$ is the 4×4 matrix and its elements $e^i_{jk}(r)$ are, referring to the solutions of equations of motion obtained by SEZAWA (1932), given by

$$(e^i_{jk})=\begin{pmatrix} h_ir j'_n(h_ir) & N^2 j_n(k_ir) & h_ir n'_n(h_ir) & N^2 n_n(k_ir)\\ j_n(h_ir) & k_ir j'_n(k_ir)+j_n(k_ir) & n_n(h_ir) & k_ir n'_n(k_ir)+n_n(k_ir)\\ \mu_i g(j_n, h_ir) & \mu_i N^2 f(j_n, k_ir) & \mu_i g(n_n, h_ir) & \mu_i N^2 f(n_n, k_ir)\\ \mu_i f(j_n, h_ir) & \mu_i h(j_n, k_ir) & \mu_i f(n_n, h_ir) & \mu_i h(n_n, k_ir)\end{pmatrix} \tag{2.4}$$

where $j_n(\zeta_ir)$ and $n_n(\zeta_ir)$ are the spherical Bessel and the spherical Neumann function of the order n respectively, h_i and k_i the wave numbers of P and S waves in the i-th layer, μ_i the rigidity, and

$$\begin{aligned}&N^2=n(n+1)\ ,\quad z'_n(\zeta_ir)=dz_n(\zeta_ir)/d(\zeta_ir) \quad (\zeta_i=h_i \text{ or } k_i)\ ,\\ &f(z_n,\ \zeta_ir)=2\zeta_ir z'_n(\zeta_ir)-2z_n(\zeta_ir)\ ,\end{aligned}$$

$$g(z_n, \zeta_i r) = -4\zeta_i r z_n'(\zeta_i r) - \{(k_i r)^2 - 2N^2\} z_n(\zeta_i r) ,$$
$$h(z_n, k_i r) = f(z_n, k_i r) + g(z_n, k_i r) . \tag{2.5}$$

The elements of the vector $\boldsymbol{c}_i$ are unknown constants in the i-th layer, which are to be determined from boundary conditions and source conditions.

From the physical requirement that displacement components have to be finite at the center of the Earth, we put, for the innermost layer, all the terms that the spherical Neumann function is concerned with to be zero. Hence, we have

$$\begin{aligned} &e^1_{j3} = e^1_{j4} = 0 \quad (j=1, 2, 3, 4) , \\ &C_1 = D_1 = 0 . \end{aligned} \tag{2.6}$$

In the liquid medium, the rigidity is zero and a shear stress vanishes. Hence we put, for $i = K+1, K+2, \cdots, L$,

$$\begin{aligned} &B_i = D_i = 0 , \\ &e^i_{j2} = e^i_{j4} = 0 \quad (j=1, 2, 3, 4) , \quad e^i_{4k} = 0 \quad (k=1, 3) , \\ &e^i_{31} = -\lambda_i (h_i r)^2 j_n(h_i r) , \quad e^i_{33} = -\lambda_i (h_i r)^2 n_n(h_i r) , \quad (r_{i-1} \leq r \leq r_i) . \end{aligned} \tag{2.7}$$

e^i_{31} and e^i_{33} are rewritten by use of λ_i (Lamé elastic parameter). Here we introduce the following notations

$$\begin{aligned} &\boldsymbol{E}^{jk}_i(r) = \begin{pmatrix} e^i_{j1} & e^i_{j2} & e^i_{j3} & e^i_{j4} \\ e^i_{k1} & e^i_{k2} & e^i_{k3} & e^i_{k4} \end{pmatrix} , \quad \hat{\boldsymbol{E}}_i(r) = \begin{pmatrix} e^i_{11} & e^i_{13} \\ e^i_{31} & e^i_{33} \end{pmatrix} , \\ &\boldsymbol{E}^j_i(r) = (e^i_{j1}, e^i_{j2}, e^i_{j3}, e^i_{j4}) , \quad \hat{\boldsymbol{c}}_i = \begin{pmatrix} A_i \\ C_i \end{pmatrix} , \end{aligned} \tag{2.8}$$

Then, the boundary conditions that displacement and stress components are continuous at each interface lead to

$$\begin{aligned} &\boldsymbol{E}_i(r_i)\boldsymbol{c}_i = \boldsymbol{E}_{i+1}(r_i)\boldsymbol{c}_{i+1} \quad (i=1, 2, \cdots, K-1, L+1, L+2, \cdots, M-1) , \\ &\hat{\boldsymbol{E}}_i(r_i)\hat{\boldsymbol{c}}_i = \hat{\boldsymbol{E}}_{i+1}(r_i)\hat{\boldsymbol{c}}_{i+1} \quad (i=K+1, K+2, \cdots, L-1) , \\ &\boldsymbol{E}^{13}_K(r_K)\boldsymbol{c}_K = \hat{\boldsymbol{E}}_{K+1}(r_K)\hat{\boldsymbol{c}}_{K+1} , \quad \boldsymbol{E}^4_K(r_K)\boldsymbol{c}_K = 0 , \\ &\hat{\boldsymbol{E}}_L(r_L)\hat{\boldsymbol{c}}_L = \boldsymbol{E}^{13}_{L+1}(r_L)\boldsymbol{c}_{L+1} , \quad \boldsymbol{E}^4_{L+1}(r_L)\boldsymbol{c}_{L+1} = 0 . \end{aligned} \tag{2.9}$$

With the aid of the first relation of Eq. (2.9), it is possible to connect the vector $\boldsymbol{c}_M$ with $\boldsymbol{c}_{L+1}$ and the vector $\boldsymbol{c}_K$ with $\boldsymbol{c}_1$. Then, putting stress components on the free surface ($r = r_M = a$) to be zero, we get

$$\boldsymbol{y}_M(a) = (aU_M(a), aV_M(a), 0, 0)^T = \boldsymbol{F}_M \boldsymbol{c}_{L+1} , \tag{2.10}$$

where

$$\boldsymbol{F}_M = \boldsymbol{D}_M \boldsymbol{D}_{M-1} \cdots\cdots \boldsymbol{D}_{L+2} \boldsymbol{E}_{L+1}(r_{L+1}) , \tag{2.11}$$

and

$$\boldsymbol{D}_i = \boldsymbol{E}_i(r_i)\boldsymbol{E}_i^{-1}(r_{i-1}) \ . \tag{2.12}$$

$\boldsymbol{E}_i^{-1}$ is the inverse matrix of $\boldsymbol{E}_i$. The other relation is

$$\boldsymbol{c}_K = \boldsymbol{F}_K \boldsymbol{c}_1 \ , \tag{2.13}$$

where

$$\boldsymbol{F}_K = \boldsymbol{E}_K^{-1}(r_{K-1})\boldsymbol{D}_{K-1}\boldsymbol{D}_{K-2}\cdots\cdots\boldsymbol{D}_2\boldsymbol{E}_1(r_1) \ . \tag{2.14}$$

In a similar manner, from the second relation of Eq. (2.9), we get

$$\hat{\boldsymbol{c}}_L = \hat{\boldsymbol{F}}_L \hat{\boldsymbol{c}}_{K+1} \ , \tag{2.15}$$

where

$$\hat{\boldsymbol{F}}_L = \hat{\boldsymbol{E}}_L^{-1}(r_{L-1})\hat{\boldsymbol{D}}_{L-1}\hat{\boldsymbol{D}}_{L-2}\cdots\cdots\hat{\boldsymbol{D}}_{K+2}\hat{\boldsymbol{E}}_{K+1}(r_{K+1}) \ . \tag{2.16}$$

A matrix with a hat means a 2×2 matrix. From the latter four equations of Eq. (2.9) and Eqs. (2.10), (2.13), (2.15), we obtain

$$\begin{aligned}
&\boldsymbol{E}_K^4(r_K)\boldsymbol{F}_K\boldsymbol{c}_1 = 0 \ , \quad \boldsymbol{E}_K^{13}(r_K)\boldsymbol{F}_K\boldsymbol{c}_1 - \hat{\boldsymbol{E}}_{K+1}(r_K)\hat{\boldsymbol{c}}_{K+1} = \hat{\boldsymbol{0}} \ , \\
&\hat{\boldsymbol{E}}_L(r_L)\hat{\boldsymbol{F}}_L\hat{\boldsymbol{c}}_{K+1} - \boldsymbol{E}_{L+1}^{13}(r_L)\boldsymbol{c}_{L+1} = \hat{\boldsymbol{0}} \ , \quad \boldsymbol{E}_{L+1}^4(r_L)\boldsymbol{c}_{L+1} = 0 \ , \\
&\boldsymbol{F}_M^{34}\boldsymbol{c}_{L+1} = \hat{\boldsymbol{0}} \ ,
\end{aligned} \tag{2.17}$$

where $\hat{\boldsymbol{0}}$ denotes the zero vector in two dimensions, and $\boldsymbol{F}_M^{34}$ is the 2×4 matrix consisting of the third and fourth rows of the matrix $\boldsymbol{F}_M$, defined in a similar manner as $\boldsymbol{E}_i^{jk}$ in Eq. (2.8). These equations can be arranged in one equational form as

$$\boldsymbol{A}\boldsymbol{c} = \boldsymbol{0} \tag{2.18}$$

where

$$\begin{aligned}
&\boldsymbol{A} = (a_{jk}) \quad (j, k = 1, 2, \cdots, 8) \ , \\
&\boldsymbol{c} = (A_1, B_1, A_{K+1}, C_{K+1}, A_{L+1}, B_{L+1}, C_{L+1}, D_{L+1})^T
\end{aligned} \tag{2.19}$$

and $\boldsymbol{0}$ means the zero vector in eight dimensions. The elements of the matrix $\boldsymbol{A}$ are given by

$$\begin{aligned}
&(a_{11}, a_{12}, 0, 0) = \boldsymbol{E}_K^4(r_K)\boldsymbol{F}_K \ , \quad \begin{pmatrix} a_{23} & a_{24} \\ a_{33} & a_{34} \end{pmatrix} = -\hat{\boldsymbol{E}}_{K+1}(r_K) \\
&\begin{pmatrix} a_{21} & a_{22} & 0 & 0 \\ a_{31} & a_{32} & 0 & 0 \end{pmatrix} = \boldsymbol{E}_K^{13}(r_K)\boldsymbol{F}_K \ , \quad \begin{pmatrix} a_{43} & a_{44} \\ a_{53} & a_{54} \end{pmatrix} = \hat{\boldsymbol{E}}_L(r_L)\hat{\boldsymbol{F}}_L \ , \\
&\begin{pmatrix} a_{45} & a_{46} & a_{47} & a_{48} \\ a_{55} & a_{56} & a_{57} & a_{58} \end{pmatrix} = -\boldsymbol{E}_{L+1}^{13}(r_L) \ , \quad (a_{65}, a_{66}, a_{67}, a_{68}) = \boldsymbol{E}_{L+1}^4(r_L) \\
&\begin{pmatrix} a_{75} & a_{76} & a_{77} & a_{78} \\ a_{85} & a_{86} & a_{87} & a_{88} \end{pmatrix} = \boldsymbol{F}_M^{34} .
\end{aligned} \tag{2.20}$$

Other elements are all identically zero.

Hence, the frequency equation of the spheroidal oscillations of the spherically symmetric, multi-layered (solid-liquid-solid) Earth is formally given as

$$\det A = 0 \ . \tag{2.21}$$

Among 8×8 elements of the matrix A, thirty components are identically zero and thus it is easy to reduce its dimension to a lower one, say, 4×4.

In obtaining the eigenfunctions, $U(r)$, $V(r)$, we have to get values of the constants $\boldsymbol{c}_i$ for all layers. This can be done as follows. If we standardize, in a conventional way, the radial component of surface displacements to be unity, that is, $U_M(a)=1$, we get another equation, from Eq. (2.10),

$$\boldsymbol{F}_M^1 \boldsymbol{c}_{L+1} = a \ , \tag{2.22}$$

where $\boldsymbol{F}_M^1$ is the row vector consisting of the first row of the matrix $\boldsymbol{F}_M$. Then we can solve the equations, (2.18) and (2.22), for $\boldsymbol{c}_1$, $\hat{\boldsymbol{c}}_{K+1}$ and $\boldsymbol{c}_{L+1}$, and subsequently Eq. (2.9) for all $\boldsymbol{c}_i$. Hence, from Eq. (2.2), we can obtain the eigenfunction $\boldsymbol{y}(r)$ for the whole space in the Earth.

A similar treatment is possible for the problem of excitation of free oscillations of the Earth due to an external force (say, a double couple point source) in it. Then, we introduce an equivalent source function (USAMI *et al.*, 1970), which is defined as a discontinuity of $\boldsymbol{y}_m(r)$ across the source surface ($r=r_s$) situated in the m-th layer. This imposes another boundary condition on $\boldsymbol{y}_i(r)$ besides Eq. (2.9). Hence, the problem has to be solved so that $\boldsymbol{y}_i(r)$ may have a jump by an amount $\delta\boldsymbol{y}_s$ (equivalent source function) at $r=r_s$ in the m-th layer. Then, it is found that Eq. (2.10) is modified to

$$(a\,U_M(a),\ a\,V_M(a),\ 0,\ 0)^T = \boldsymbol{F}_M \boldsymbol{c}_{L+1} + \boldsymbol{F}_s \boldsymbol{E}_m^{-1}(r_s)\delta\boldsymbol{y}_s \ , \tag{2.23}$$

where

$$\boldsymbol{F}_s = \boldsymbol{D}_M \boldsymbol{D}_{M-1} \cdots \boldsymbol{D}_{m+1} \boldsymbol{E}_m(r_m) \ . \tag{2.24}$$

If we put the source term as

$$\boldsymbol{F}_s \boldsymbol{E}_m^{-1}(r_s)\delta\boldsymbol{y}_s = \boldsymbol{f}^s = (f_1^s,\ f_2^s,\ f_3^s,\ f_4^s)^T \ , \tag{2.25}$$

we get, in place of the last relation of Eq. (2.17),

$$\boldsymbol{F}_M^{34} \boldsymbol{c}_{L+1} = -(f_3^s,\ f_4^s)^T \ , \tag{2.26}$$

and thus, in place of Eq. (2.18),

$$\boldsymbol{Ac}=(0,\ 0,\ 0,\ 0,\ 0,\ 0,\ -f_3^s,\ -f_4^s)^T\ . \tag{2.27}$$

By solving these simultaneous linear equations we can get the constants $\boldsymbol{c}_1$, $\hat{\boldsymbol{c}}_{K+1}$ and $\boldsymbol{c}_{L+1}$. Hence, the formal solution for surface displacements is readily obtained from Eq. (2.23).

When an Earth consists of solid (crust/mantle) and liquid (core) media, we have only to remove the inner solid layers from the preceding model. Then, the $(K+1)st$ layer is shifted to the lowest layer which includes the center of the Earth, and we put $e_{13}^{K+1}=e_{33}^{K+1}=0$, $C_{K+1}=0$ in the same manner as Eq. (2.6). Slight modification of the preceding formulation leads, instead of Eq. (2.18), to

$$\begin{pmatrix} a_{43} & a_{45} & a_{46} & a_{47} & a_{48} \\ a_{53} & a_{55} & a_{56} & a_{57} & a_{58} \\ 0 & a_{65} & a_{66} & a_{67} & a_{68} \\ 0 & a_{75} & a_{76} & a_{77} & a_{78} \\ 0 & a_{85} & a_{86} & a_{87} & a_{88} \end{pmatrix} \begin{pmatrix} A_{K+1} \\ A_{L+1} \\ B_{L+1} \\ C_{L+1} \\ D_{L+1} \end{pmatrix} = \begin{pmatrix} 0 \\ 0 \\ 0 \\ 0 \\ 0 \end{pmatrix} \tag{2.28}$$

where the elements a_{jk} are the same as those defined in Eq. (2.20). The frequency equation is given by the determinant of the above matrix $\tilde{A}$, that is,

$$\det \tilde{A} = 0\ , \tag{2.29}$$

where

$$\tilde{A}=(a_{jk}) \quad \begin{pmatrix} j=4,\ 5,\ \cdots,\ 8 \\ k=3,\ 5,\ \cdots,\ 8 \end{pmatrix}\ . \tag{2.30}$$

When an Earth is constructed by only solid layers, we remove the liquid and inner solid layers from the first model. Then, the $(L+1)$st layer is shifted to the lowest one and we have to put $e_{j3}^{L+1}=e_{j4}^{L+1}=0$ $(j=1,\ 2,\ 3,\ 4)$, $C_{L+1}=D_{L+1}=0$. In this case, the last equation of (2.17) can be rewritten as

$$\begin{pmatrix} f_{31}^M & f_{32}^M \\ f_{41}^M & f_{42}^M \end{pmatrix} \begin{pmatrix} A_{L+1} \\ B_{L+1} \end{pmatrix} = \begin{pmatrix} 0 \\ 0 \end{pmatrix} \tag{2.31}$$

where f_{jk}^M is an element of the matrix $\boldsymbol{F}_M$. Hence, the frequency equation is simply given as

$$f_{31}^M f_{42}^M - f_{32}^M f_{41}^M = 0\ . \tag{2.32}$$

3. Asymptotic Frequency Equation

When an argument of the spherical Bessel (or Neumann) function

is very large compared with its order, $j_n(z)$ and $n_n(z)$ are asymptotically approximated as (Watson 1952, p. 199)

$$j_n(z) \simeq (1/z)\sin(z-n\pi/2)\ , \quad n_n(z) \simeq -(1/z)\cos(z-n\pi/2)\ .$$

Hence, if we assume $h_i r \gg n$ ($r \geq r_1$, $i=1, 2, \cdots, M$), we have the following approximations for the functions in $\boldsymbol{E}_i(r)$

$$\begin{aligned} &j_n(z) \simeq (1/z)\sin Z\ , \quad n_n(z) \simeq -(1/z)\cos Z\ , \\ &j'_n(z) \simeq (1/z)\cos Z\ , \quad n'_n(z) \simeq (1/z)\sin Z\ , \\ &f(j_n, z) \simeq 2\cos Z\ , \quad g(j_n, z) \simeq -(z_k^2/z)\sin Z\ , \quad h(j_n, z_k) \simeq -z_k \sin Z_k\ , \\ &f(n_n, z) \simeq 2\sin Z\ , \quad g(n_n, z) \simeq (z_k^2/z)\cos Z\ , \quad h(n_n, z_k) \simeq z_k \cos Z_k\ , \end{aligned} \tag{3.1}$$

where

$$z = h_i r \quad \text{or} \quad k_i r\ , \quad z_k = k_i r\ , \quad Z = z - n\pi/2\ , \quad Z_k = z_k - n\pi/2\ .$$

Substituting the above formulas into Eq. (2.4), and keeping the most predominant terms, we get

$$\boldsymbol{E}_i(r) \simeq \begin{pmatrix} \cos H_r^i & 0 & \sin H_r^i & 0 \\ 0 & \cos K_r^i & 0 & \sin K_r^i \\ -\omega\rho_i\alpha_i r \sin H_r^i & 0 & \omega\rho_i\alpha_i r \cos H_r^i & 0 \\ 0 & -\omega\rho_i\beta_i r \sin K_r^i & 0 & \omega\rho_i\beta_i r \cos K_r^i \end{pmatrix} . \tag{3.2}$$

where

$$H_r^i = h_i r - n\pi/2,\ K_r^i = k_i r - n\pi/2\ , \tag{3.3}$$

and ρ_i, α_i and β_i mean the density, P and S wave velocities in the i-th layer respectively, and ω the angular frequency. During reduction, the relations $\mu_i(k_i r)^2/(h_i r) = \omega\rho_i\alpha_i r$, $\mu_i k_i r = \omega\rho_i\beta_i r$ are employed. Thus, the matrix $\boldsymbol{E}_i(r)$ is reduced to a very simple form, and its inverse matrix is immediately obtained as

$$\boldsymbol{E}_i^{-1}(r) \simeq \begin{pmatrix} \cos H_r^i & 0 & -(1/\omega\rho_i\alpha_i r)\sin H_r^i & 0 \\ 0 & \cos K_r^i & 0 & -(1/\omega\rho_i\beta_i r)\sin K_r^i \\ \sin H_r^i & 0 & (1/\omega\rho_i\alpha_i r)\cos H_r^i & 0 \\ 0 & \sin K_r^i & 0 & (1/\omega\rho_i\beta_i r)\cos K_r^i \end{pmatrix} \tag{3.4}$$

Hence, we have, from Eq. (2.12),

$$\boldsymbol{D}_i \simeq \begin{pmatrix} \cos h_i d_i & 0 & (1/\omega\rho_i\alpha_i r_{i-1})\sin h_i d_i & 0 \\ 0 & \cos k_i d_i & 0 & (1/\omega\rho_i\beta_i r_{i-1})\sin k_i d_i \\ -\omega\rho_i\alpha_i r_i \sin h_i d_i & 0 & (r_i/r_{i-1})\cos h_i d_i & 0 \\ 0 & -\omega\rho_i\beta_i r_i \sin k_i d_i & 0 & (r_i/r_{i-1})\cos k_i d_i \end{pmatrix} \tag{3.5}$$

where $d_i = r_i - r_{i-1}$ (thickness of the i-th layer).

If we write a term associated with P wave as "P" and that with S wave as "S", we find that $\boldsymbol{E}_i$, $\boldsymbol{E}_i^{-1}$ and $\boldsymbol{D}_i$ are all denoted formally as

$$\begin{pmatrix} P & 0 & P & 0 \\ 0 & S & 0 & S \\ P & 0 & P & 0 \\ 0 & S & 0 & S \end{pmatrix} \tag{3.6}$$

Then, it is readily proved that $\boldsymbol{F}_M$ and $\boldsymbol{F}_K$ also retain a similar matrix form as (3.6). All the elements of $\hat{\boldsymbol{F}}_L$ are naturally identified as "P". In the result, each element a_{jk} in Eq. (2.20) is expressed in its asymptotic form as

$$\begin{aligned} &a_{11} \simeq 0,\ a_{12} \simeq S_1^K,\ a_{21} \simeq P_1^K,\ a_{22} \simeq 0,\ a_{31} \simeq P_2^K,\ a_{32} \simeq 0,\ a_{23} \simeq P_1^L,\ a_{24} \simeq P_2^L\ , \\ &a_{33} \simeq P_3^L,\ a_{34} \simeq P_4^L,\ a_{43} \simeq P_5^L,\ a_{44} \simeq P_6^L,\ a_{53} \simeq P_7^L,\ a_{54} \simeq P_8^L\ , \\ &a_{45} \simeq P_1^M,\ a_{46} \simeq 0,\ a_{47} \simeq P_2^M,\ a_{48} \simeq 0,\ a_{55} \simeq P_3^M,\ a_{56} \simeq 0,\ a_{57} \simeq P_4^M,\ a_{58} \simeq 0\ , \\ &a_{65} \simeq 0,\ a_{66} \simeq S_1^M,\ a_{67} \simeq 0,\ a_{68} \simeq S_2^M,\ a_{75} \simeq P_5^M,\ a_{76} \simeq 0,\ a_{77} \simeq P_6^M,\ a_{78} \simeq 0\ , \\ &a_{85} \simeq 0,\ a_{86} \simeq S_3^M,\ a_{87} \simeq 0,\ a_{88} \simeq S_4^M\ , \end{aligned} \tag{3.7}$$

where the symbols "P" and "S" mean that an element is connected with P and S waves respectively and the superscripts K, L and M discriminate elements which are associated with the inner core, outer core and crust/mantle respectively. The numerical subscripts are merely put in order of appearance.

Now, Eq. (2.21) is formally reduced to

$$\det \begin{pmatrix} 0 & S_1^K & 0 & 0 & & & & \\ P_1^K & 0 & P_1^L & P_2^L & & & 0 & \\ P_2^K & 0 & P_3^L & P_4^L & & & & \\ 0 & 0 & P_5^L & P_6^L & P_1^M & 0 & P_2^M & 0 \\ 0 & 0 & P_7^L & P_8^L & P_3^M & 0 & P_4^M & 0 \\ & & & & 0 & S_1^M & 0 & S_2^M \\ & 0 & & & P_5^M & 0 & P_6^M & 0 \\ & & & & 0 & S_3^M & 0 & S_4^M \end{pmatrix} = 0\ . \tag{3.8}$$

Further reduction yields three independent equations,

$$S_1^K = 0\ , \qquad \det\begin{pmatrix} S_1^M & S_2^M \\ S_3^M & S_4^M \end{pmatrix} = 0\ , \quad \det\begin{pmatrix} P_1^K & P_1^L & P_2^L & 0 & 0 \\ P_2^K & P_3^L & P_4^L & 0 & 0 \\ 0 & P_5^L & P_6^L & P_1^M & P_2^M \\ 0 & P_7^L & P_8^L & P_3^M & P_4^M \\ 0 & 0 & 0 & P_5^M & P_6^M \end{pmatrix} = 0\ . \tag{3.9}$$

The first, second and third equations give eigenfrequencies for shear oscillations of the inner solid sphere (inner core), shear oscillations of the outer solid shell (crust/mantle) and compressional oscillations of the whole Earth respectively. These three modes are called J, $(ScS)_V$ and $PKIKP$ type respectively, corresponding to three different body-wave types (ANDERRSEN *et al.*, 1975; GILBERT, 1975). This decoupling of the rays is possible only for their radial propagation in the Earth because no conversion of wave types occurs at a boundary in the Earth for their normal incidence on it and they behave independently there. In view of the mode-ray duality (BEN-MENAHEM, 1964a), it is found that the basic assumption in this section that $h_i r \gg n$ (*i.e.*, the phase velocity is very high) just fits this ray-geometrical condition.

For the Earth consisting of solid (crust/mantle) and liquid (core) media, Eq. (2.29) is available instead of (2.21). Hence, the asymptotic frequency equation (3.9) reduces to

$$\det\begin{pmatrix} S_1^M & S_2^M \\ S_3^M & S_4^M \end{pmatrix}=0\ , \quad \det\begin{pmatrix} P_5^L & P_1^M & P_2^M \\ P_7^L & P_3^M & P_4^M \\ 0 & P_5^M & P_6^M \end{pmatrix}=0\ . \tag{3.10}$$

GILBERT (1975) has proved the decoupling of a frequency equation at high frequency directly from decomposition of basic differential equations for elastic material. His paper does not, however, include investigation on the effect of discontinuities in the medium on eigenfrequencies. In the following part, we derive the asymptotic frequency equations in explicit forms for simple Earth models, consisting of a uniform liquid core and a small number of solid spherical layers overlying it. Hereafter, we will call the $(ScS)_V$ type modes simply as "*ScS*-type" and *PKIKP* type as "*PKP*-type" (due to nonexistence of inner core phase), corresponding to the two equations of Eq. (3.10) respectively.

Since we assume the uniform liquid core, the L-th layer in Fig. 1 is reduced to the first layer. Hence, we put $L=1$ in the previous equations. Then, the layer 1 and r_1 indicate the uniform liquid core and its radius. Each element in Eq. (3.10) is obtained from Eqs. (2.15), (2.16), (2.20), (3.2) and (3.7), so we have

$$\begin{aligned}
a_{43} &= e_{11}^1(r_1) \simeq \cos H_{r1}^1 = P_5^L\ , \\
a_{53} &= e_{31}^1(r_1) \simeq -\omega\rho_1\alpha_1 r_1 \sin H_{r1}^1 = P_7^L\ , \\
a_{45} &= -e_{11}^2(r_1) \simeq -\cos H_{r1}^2 = P_1^M\ , \\
a_{47} &= -e_{13}^2(r_1) \simeq -\sin H_{r1}^2 = P_2^M\ , \\
a_{55} &= -e_{31}^2(r_1) \simeq \omega\rho_2\alpha_2 r_1 \sin H_{r1}^2 = P_3^M\ ,
\end{aligned}$$

$$
\begin{aligned}
a_{57} &= -e_{33}^2(r_1) \simeq -\omega\rho_2\alpha_2 r_1 \cos H_{r1}^2 = P_4^M \ , \\
a_{66} &= e_{42}^2(r_1) \simeq -\omega\rho_2\beta_2 r_1 \sin K_{r1}^2 = S_1^M \ , \\
a_{68} &= e_{44}^2(r_1) \simeq \omega\rho_2\beta_2 r_1 \cos K_{r1}^2 = S_2^M \ ,
\end{aligned} \tag{3.11}
$$

where

$$
H_{rj}^i = h_i r_j - n\pi/2 \ , \quad K_{rj}^i = k_i r_j - n\pi/2 \quad (j = i \text{ or } i-1) \tag{3.12}
$$

These elements are common to any model with a uniform liquid core. The other elements, P_5^M, P_6^M, S_3^M, S_4^M, are obtained from an asymptotic formula for $\boldsymbol{F}_M^{34}$, which depends on the number of layers overlying the core. For brevity's sake, we introduce the notations

$$
\begin{aligned}
R_i^P &= (\rho_{i+1}\alpha_{i+1} - \rho_i\alpha_i)/(\rho_{i+1}\alpha_{i+1} + \rho_i\alpha_i) \ , \\
R_i^S &= (\rho_{i+1}\beta_{i+1} - \rho_i\beta_i)/(\rho_{i+1}\beta_{i+1} + \rho_i\beta_i) \ ,
\end{aligned} \tag{3.13}
$$

which are the reflection coefficients for normal incidence of P and S waves on the i-th interface respectively.

(i) Two-Layered Model (a homogeneous mantle and liquid core) From Eqs. (2.11), (2.20), (3.2) and (3.7), we get

$$
\begin{aligned}
a_{75} &= e_{31}^2(r_2) \simeq -\omega\rho_2\alpha_2 r_2 \sin H_{r2}^2 = P_5^M \ , \\
a_{77} &= e_{33}^2(r_2) \simeq \omega\rho_2\alpha_2 r_2 \cos H_{r2}^2 = P_6^M \ , \\
a_{86} &= e_{42}^2(r_2) \simeq -\omega\rho_2\beta_2 r_2 \sin K_{r2}^2 = S_3^M \ , \\
a_{88} &= e_{44}^2(r_2) \simeq \omega\rho_2\beta_2 r_2 \cos K_{r2}^2 = S_4^M \ .
\end{aligned} \tag{3.14}
$$

Inserting Eqs. (3.11) and (3.14) into (3.10) and arranging it, we get

$$
\begin{aligned}
&\sin k_2 d_2 = 0 \ , \\
&\sin(h_2 d_2 + h_1 r_1 - n\pi/2) + R_1^P \sin(h_2 d_2 - h_1 r_1 + n\pi/2) = 0 \ .
\end{aligned} \tag{3.15}
$$

The first equation is the asymptotic frequency equation for the *ScS*-type modes and the second one is for the *PKP*-type modes.

(ii) Three-Layered Model (a two-layered mantle and a liquid core) From Eq. (2.11), we have

$$
\boldsymbol{F}_M = \boldsymbol{D}_3 \boldsymbol{E}_2(r_2) \ . \tag{3.16}
$$

Then, with the aid of Eqs. (2.20), (3.2), (3.5) and (3.7), we obtain

$$
\begin{aligned}
a_{75} &\simeq -\omega\rho_3\alpha_3 r_3 \sin h_3 d_3 \cos H_{r2}^2 + (r_3/r_2)(P_5^M)_{\mathrm{i}} \cos h_3 d_3 = P_5^M \ , \\
a_{77} &\simeq -\omega\rho_3\alpha_3 r_3 \sin h_3 d_3 \sin H_{r2}^2 + (r_3/r_2)(P_6^M)_{\mathrm{i}} \cos h_3 d_3 = P_6^M \ , \\
a_{86} &\simeq -\omega\rho_3\beta_3 r_3 \sin k_3 d_3 \cos K_{r2}^2 + (r_3/r_2)(S_3^M)_{\mathrm{i}} \cos k_3 d_3 = S_3^M \ , \\
a_{88} &\simeq -\omega\rho_3\beta_3 r_3 \sin k_3 d_3 \sin K_{r2}^2 + (r_3/r_2)(S_4^M)_{\mathrm{i}} \cos k_3 d_3 = S_4^M \ ,
\end{aligned} \tag{3.17}
$$

where $(P_5^M)_{\mathrm{i}}$, $(P_6^M)_{\mathrm{i}}$, $(S_3^M)_{\mathrm{i}}$ and $(S_4^M)_{\mathrm{i}}$ are the coefficients defined for the preceding case and are identical with P_5^M, P_6^M, S_3^M and S_4^M in Eq. (3.14)

respectively.

Substitution of Eqs. (3.11) and (3.17) into (3.10) leads to, corresponding to the *ScS*-type and *PKP*-type respectively,

$$\begin{aligned}
&\sin(k_3d_3+k_2d_2)+R_2^S\sin(k_3d_3-k_2d_2)=0\ ,\\
&\sin(h_3d_3+h_2d_2+h_1r_1-n\pi/2)+R_1^P\sin(h_3d_3+h_2d_2-h_1r_1+n\pi/2)\\
&+R_2^P\sin(h_3d_3-h_2d_2-h_1r_1+n\pi/2)+R_2^PR_1^P\sin(h_3d_3-h_2d_2+h_1r_1-n\pi/2)\\
&=0\ ,
\end{aligned}\tag{3.18}$$

where R_i^P and R_i^S are the reflection coefficients defined by Eq. (3.13), and d_i is the thickness of the i-th layer.

(iii) Four-Layered Model (a three-layered mantle and a liquid core) From Eq. (2.11), we have

$$\boldsymbol{F}_M=\boldsymbol{D}_4\boldsymbol{D}_3\boldsymbol{E}_2(r_2)\ ,\tag{3.19}$$

which yields, through Eqs. (2.20), (3.2), (3.5) and (3.7),

$$\begin{aligned}
a_{75}\simeq&-\omega\rho_4\alpha_4r_4\sin h_4d_4\{\cos h_3d_3\cos H_{r2}^2-(\rho_2\alpha_2/\rho_3\alpha_3)\sin h_3d_3\sin H_{r2}^2\}\\
&+(r_4/r_3)(P_5^M)_{11}\cos h_4d_4=P_5^M\ ,\\
a_{77}\simeq&-\omega\rho_4\alpha_4r_4\sin h_4d_4\{\cos h_3d_3\sin H_{r2}^2+(\rho_2\alpha_2/\rho_3\alpha_3)\sin h_3d_3\cos H_{r2}^2\}\\
&+(r_4/r_3)(P_6^M)_{11}\cos h_4d_4=P_6^M\ ,\\
a_{86}\simeq&-\omega\rho_4\beta_4r_4\sin k_4d_4\{\cos k_3d_3\cos K_{r2}^2-(\rho_2\beta_2/\rho_3\beta_3)\sin k_3d_3\sin K_{r2}^2\}\\
&+(r_4/r_3)(S_3^M)_{11}\cos k_4d_4=S_3^M\ ,\\
a_{88}\simeq&-\omega\rho_4\beta_4r_4\sin k_4d_4\{\cos k_3d_3\sin K_{r2}^2+(\rho_2\beta_2/\rho_3\beta_3)\sin k_3d_3\cos K_{r2}^2\}\\
&+(r_4/r_3)(S_4^M)_{11}\cos k_4d_4=S_4^M\ ,
\end{aligned}\tag{3.20}$$

where $(P_5^M)_{11}$, $(P_6^M)_{11}$, $(S_3^M)_{11}$ and $(S_4^M)_{11}$ stand for the coefficients P_5^M, P_6^M, S_3^M and S_4^M in Eq. (3.17).

After substitution of Eqs. (3.11) and (3.20) into (3.10) and some algebraic manipulations, we get

$$\begin{aligned}
&\sin(\eta_4+\eta_3+\eta_2)+R_2^S\sin(\eta_4+\eta_3-\eta_2)+R_3^S\sin(\eta_4-\eta_3-\eta_2)\\
&\qquad+R_3^SR_2^S\sin(\eta_4-\eta_3+\eta_2)=0\ ,\\
&\sin(\xi_4+\xi_3+\xi_2+H_{r1}^1)+R_1^P\sin(\xi_4+\xi_3+\xi_2-H_{r1}^1)+R_2^P\sin(\xi_4+\xi_3-\xi_2-H_{r1}^1)\\
&\qquad+R_3^P\sin(\xi_4-\xi_3-\xi_2-H_{r1}^1)+R_2^PR_1^P\sin(\xi_4+\xi_3-\xi_2+H_{r1}^1)\\
&\qquad+R_3^PR_2^P\sin(\xi_4-\xi_3+\xi_2+H_{r1}^1)+R_3^PR_1^P\sin(\xi_4-\xi_3-\xi_2+H_{r1}^1)\\
&\qquad+R_3^PR_2^PR_1^P\sin(\xi_4-\xi_3+\xi_2-H_{r1}^1)=0\ ,
\end{aligned}\tag{3.21}$$

where η_i and ξ_i are short for k_id_i and h_id_i respectively and H_{r1}^1 for $h_1r_1-n\pi/2$. The first and second equations correspond to the *ScS*-type and *PKP*-type modes respectively.

The equations for a general M-layered Model can readily be deduced from Eqs. (3.15), (3.18) and (3.21), if we ignore the terms of higher orders than the second in the reflection coefficients.

It is found that the second equation of (3.15) and the first one of (3.18) have similar forms to each other. Moreover the second equation of (3.18) and the first one of (3.21) are similar as well. Hence we can say that the discontinuities in the medium produce a similar effect on the asymptotic frequency equations for both *ScS*-type and *PKP*-type modes when the number of the discontinuities effective for respective modes is the same (note that the mantle-core boundary acts as a free surface for the *ScS*-type modes). The only difference is that the equations for the *PKP*-type modes have different forms according as n(angular order) is even or odd, resulting from the factor $H_{r1}^{1}(=h_1 r_1 - n\pi/2)$, while those for the *ScS*-type do not depend on n. From a viewpoint of ray theory, this difference arises from the fact that the *PKP* wave now concerned crosses the sphere but the *ScS* wave does not. These circumstances will be illustrated by ODAKA (1980b).

Referring to Eq. (8.2) of SATO and LAPWOOD (1977a) and Eq. (5.3) of the same authors (1977b), we find that their equations for toroidal modes are identical with our first equations of Eqs. (3.18) and (3.21) respectively. Hence, we may conclude that eigenfrequencies of the *ScS*-type modes of the spheroidal oscillations and those of the toroidal modes are identical for the same Earth model at high frequencies, and thus internal discontinuities produce entirely the same effect on both eigenfrequencies.

4. Asymptotic Distribution of Eigenfrequencies

In describing asymptotic patterns of distribution of toroidal and spheroidal eigenfrequencies, some different formulas have been used by different authors. These formulas are mainly defined as a function of two adjacent eigenfrequencies such as $A(f_{i+1}-f_i)^{\pm 1}$, $B(f_{i+1}^2-f_i^2)^{-1/2}$. These formulas are, however, not suitable for obtaining a knowledge of absolute values of the eigenfrequencies.

Alternatively, we investigate asymptotic patterns of the following quantities defined for the *PKP*-type and *ScS*-type modes respectively by reference to the formula introduced by LAPWOOD and SATO (1977, 1978) for the torsional case.

$$\begin{aligned} S_p &= 2t_p f_i^p - (i+\varepsilon/2) \quad (i=1, 2, 3, \cdots), \\ S_s &= 2t_s f_{i'}^s - i' \quad (i'=1, 2, 3, \cdots), \end{aligned} \tag{4.1}$$

where f_i^p and $f_{i'}^s$ are the eigenfrequencies of the i-th and i'-th radial

modes of the *PKP*-type and *ScS*-type modes respectively (to be exact, i and i' shift from real mode numbers by certain integral values which depend on angular order n), t_p and t_s are the radial travel time of a *P*-ray between the surface and the center of the Earth and that of an *S*-ray between the surface and the mantle-core boundary, and $\varepsilon=0$ or 1 according as n is even or odd.

It is readily proved that the zero order approximations to solutions of Eqs. (3.15), (3.18) and (3.21), obtained by discarding all the terms multiplied by the reflection coefficients, are identically given by

$$f_i^p \simeq (i+\varepsilon/2)/2t_p\ , \quad f_{i'}^s \simeq i'/2t_s\ , \tag{4.2}$$

where i and i' are the integers.

Hence, the zero order approximations to S_p and S_s are equally reduced to zero. For this reason, the term $\varepsilon/2$ is included in the definition of S_p in Eq. (4.1). From Eq. (4.2) we get

$$f_{i+1}^p - f_i^p \simeq 1/2t_p\ , \quad f_{i'+1}^s - f_{i'}^s \simeq 1/2t_s\ . \tag{4.3}$$

This constant spacing of the eigenfrequencies results from neglecting the effect of the internal reflections. Similar formulas to Eqs. (4.2) and (4.3) have been presented by ANDERSSEN *et al.* (1975) and OKAL (1978) and checked against realistic Earth models.

We can obtain the first order approximations, allowing for the effect of reflections at the internal discontinuities, in a similar manner as attempted by LAPWOOD and SATO (1977).

From the second equation of (3.15), we get

$$S_p \simeq -(R_1^P/\pi)\sin\{2\pi(i+\varepsilon/2)t_2/t_p\}\ , \tag{4.4}$$

where $t_p = t_1 + t_2 = r_1/\alpha_1 + d_2/\alpha_2$.

From Eq. (3.18), we get

$$\begin{aligned} &S_s \simeq -(R_2^S/\pi)\sin(2\pi i' t_3'/t_s)\ , \\ &S_p \simeq (-1)^n (R_1^P/\pi)\sin\{2\pi(i+\varepsilon/2)t_1/t_p\} - (R_2^P/\pi)\sin\{2\pi(i+\varepsilon/2)t_3/t_p\}\ , \end{aligned} \tag{4.5}$$

where $t_p = t_1 + t_2 + t_3 = r_1/\alpha_1 + d_2/\alpha_2 + d_3/\alpha_3$, $t_s = t_2' + t_3' = d_2/\beta_2 + d_3/\beta_3$.

From Eq. (3.21), we get

$$\begin{aligned} &S_s \simeq (R_2^S/\pi)\sin(2\pi i' t_2'/t_s) - (R_3^S/\pi)\sin(2\pi i' t_4'/t_s)\ , \\ &S_p \simeq (-1)^n (R_1^P/\pi)\sin\{2\pi(i+\varepsilon/2)t_1/t_p\} - (R_2^P/\pi)\sin\{2\pi(i+\varepsilon/2)(t_3+t_4)/t_p\} \\ &\qquad - (R_3^P/\pi)\sin\{2\pi(i+\varepsilon/2)t_4/t_p\}\ , \end{aligned} \tag{4.6}$$

where $t_p = \sum_{k=1}^4 t_k = \sum_{k=2}^4 (d_k/\alpha_k) + (r_1/\alpha_1)$, $t_s = \sum_{k=2}^4 t_k' = \sum_{k=2}^4 (d_k/\beta_k)$.

It can be inferred from these formulas that the solutions for the *ScS*-type and *PKP*(*PKIKP*)-type modes of the *M*-layered Earth are given by

$$
\begin{aligned}
S_s &\simeq -\sum_{j=2}^{M-1} (R_j^S/\pi)\sin\left\{2\pi i'\left(\sum_{k=j+1}^{M} t_k'\right)\Big/ t_s\right\} \\
&= \sum_{j=2}^{M-1} (R_j^S/\pi)\sin\left\{2\pi i'\left(\sum_{k=2}^{j} t_k'\right)\Big/ t_s\right\}, \\
S_p &\simeq -\sum_{j=1}^{M-1} (R_j^P/\pi)\sin\left\{2\pi(i+\varepsilon/2)\left(\sum_{k=j+1}^{M} t_k\right)\Big/ t_p\right\} \\
&= (-1)^n \sum_{j=1}^{M-1} (R_j^P/\pi)\sin\left\{2\pi(i+\varepsilon/2)\left(\sum_{k=1}^{j} t_k\right)\Big/ t_p\right\},
\end{aligned}
\tag{4.7}
$$

where $t_s = \sum_{k=2}^{M} t_k' = \sum_{k=2}^{M} (d_k/\beta_k)$, $t_p = \sum_{k=1}^{M} t_k = \sum_{k=2}^{M} (d_k/\alpha_k) + (r_1/\alpha_1)$.

The exact frequency equation (2.29) contains two kinds of solutions in indefinite order which are to be classified into the *PKP*-type and *ScS*-type modes respectively at high frequencies. Hence, in investigating asymptotic behavior of the functions S_p and S_s numerically on the basis of Eqs. (2.29) and (4.1), we first have to sort out its solutions into two groups. When the scale of discontinuity (absolute value of reflection coefficient) is small, Eqs. (4.2) and (4.3) are helpful for this purpose, though they do not always work decisively. In the case of $n=0$, we do not have such difficulty since all modes are equally identified as the *PKP*-type.

We made numerical computations for three models called *LYR* 2, *LYR* 3 and *LYR* 4 (see Fig. 2), corresponding to the three cases discussed in the preceding section. Then, thickness of layers, densities and *S*-wave velocities in the mantle are designed after the spherical shell models employed by LAPWOOD and SATO (1977, 1978). This setting of the Earth structure enables us to make use of their results for the toroidal modes as information about our *ScS*-type modes of the spheroidal oscillations since the asymptotic frequency equations for these two modes must be the same as mentioned before. Thus we can get rid of uncertainty of classifying the spheroidal modes into

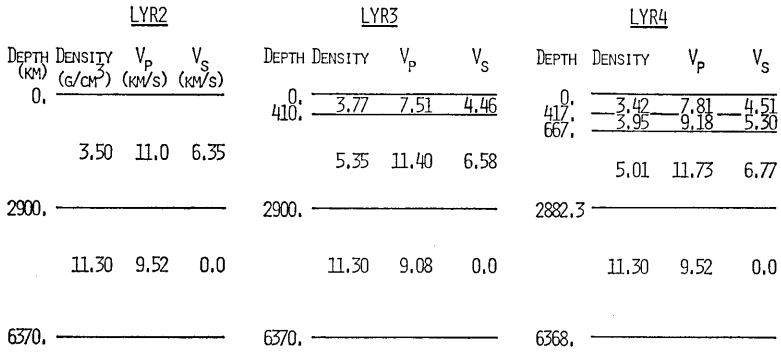

Fig. 2. Density, *P*- and *S*-wave velocity structures for two-, three- and four-layered Earth models. A liquid core is assumed for every model.

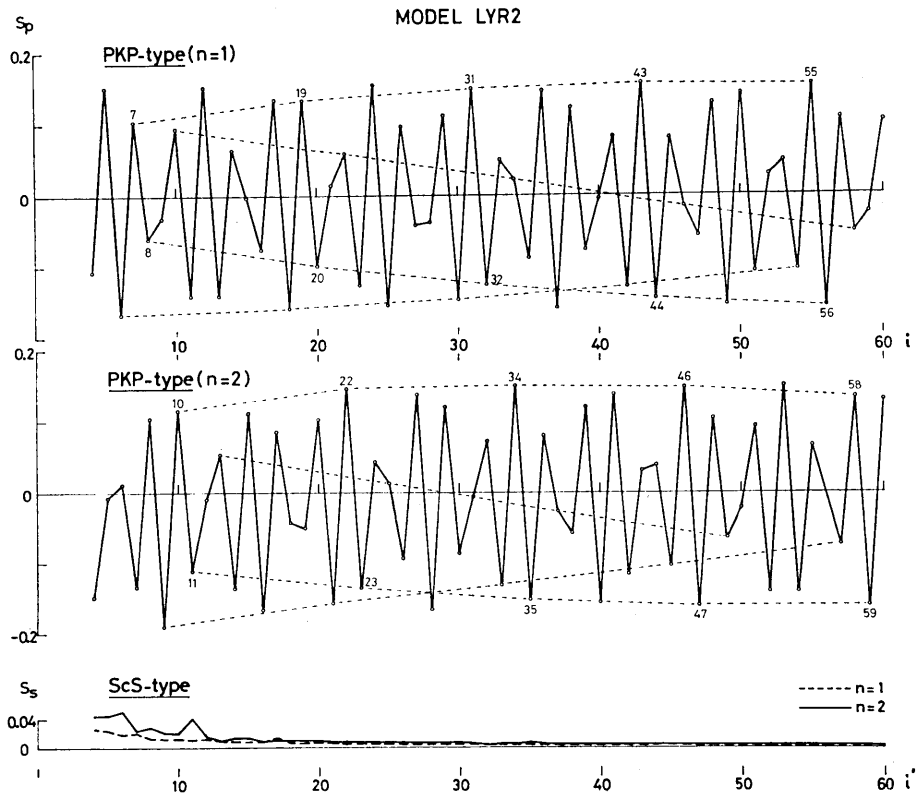

Fig. 3. Graphs of S_p against i (upper two) and S_s against i' (bottom) for the model LYR 2. Computation is made for the angular order $n=1$ and 2. Dashed curves represent the smoothly varying property of S_p at every 12 steps in i.

the *ScS*- and *PKP*-type modes. Generally speaking, for accurate classification of the modes to be made, we will have to compute such physical quantities as compressional and shear elastic energy (DZIEWONSKI and GILBERT, 1972), radial distribution of displacements (ODAKA, 1978), and phase and group velocities (OKAL, 1978).

Figure 3 shows graphs of S_p and S_s for the model LYR 2 calculated in terms of Eq. (4.1), eigenfrequencies being computed on the basis of the exact frequency equation. Discrete points plotted against integral values of i and i' are joined by solid straight lines successively. Two curves for n (angular order number)$=1$ and 2 are representative of two cases when n is odd and even respectively. As inferred from the theory, there is no significant difference in the bottom two curves of the *ScS*-type modes and their values are negligibly small compared with those of the *PKP*-type modes (note that there exists no internal discontinuity in the present model for *S*-wave

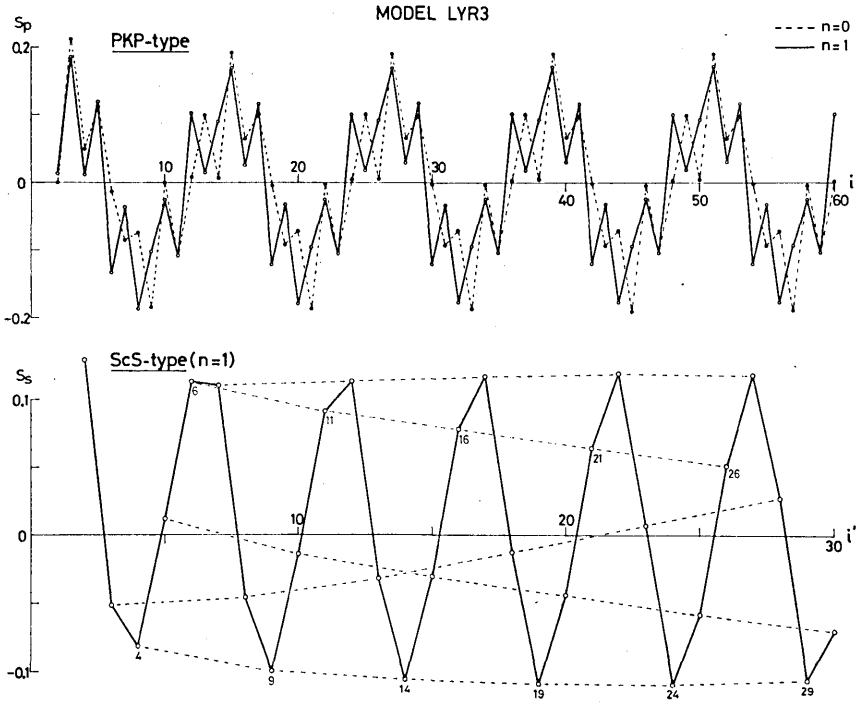

Fig. 4. Graphs of S_p against i (top) and S_s against i' (bottom) for the model *LYR* 3. Computation is made for the angular order $n=0$ (only for the *PKP*-type modes) and 1. Dashed curves for the *ScS*-type modes represent the smoothly varying property of S_s at every 5 steps in i'.

propagation). On the contrary, the curves for the *PKP*-type modes vibrate rapidly as a function of i, resulting from existence of the mantle-core boundary. Their amplitude, period and dependence on n are well illustrated in terms of Eq. (4.4), because we get, from the elastic parameters in Fig. 2, $-R_1^P/\pi$ (amplitude)$\simeq$0.15 and t_p/t_2 (period in i)$\simeq$2.4 for the present model. Broken lines indicate that successive points taken every 12 steps in i lie on a smooth sinusoidal curve, of which amplitude and period are explainable in a similar way as attempted by LAPWOOD and SATO (1977) for the toroidal case.

Computational results for the model *LYR* 3 are given in Fig. 4. The curve for the *ScS*-type modes shows a typical pattern of the so-called "solotone effect" (MCNABB *et al.*, 1976), a vibration with a single frequency, which suggests existence of single discontinuity in the medium. Its amplitude and period agree well with those expected from the approximate formula (4.5) since we get $-R_2^S/\pi$ (amplitude)$\simeq$ 0.11 and t_s/t_3' (period in i')$\simeq$5.1 for this model. Referring to Figs. 1 and 4 of LAPWOOD and SATO (1977), we find that there is a close similarity

between our curve for the *ScS*-type modes and their curve for the toroidal modes over nearly the whole range of i'. This implies that decoupling of the spheroidal modes for $n=1$ into two types of modes, *PKP* and *ScS*, begins from very low radial modes, that is, from very low frequency range.

The solid and dashed curves for the *PKP*-type modes in Fig. 4 stand for the cases $n=1$ and 0 respectively as representatives of odd and even numbers of n. It is clear that both patterns consist of the superposition of two curves with different amplitudes and periods. Their values are roughly coincident with those inferred from Eq. (4.5) since we get $-R_1^P/\pi \simeq 0.08$, $-R_2^P/\pi \simeq 0.12$, $t_p/t_1 \simeq 1.7$, $t_p/t_3 \simeq 12.0$ from the elastic parameters in Fig. 2. Thus, it is concluded that a thin surface layer gives rise to long-period oscillations(in i), while the core does short-period fluctuations and their amplitude is proportional to the scale of the corresponding discontinuities. These results are consistent with those obtaided by ANDERSSEN (1977) and WANG *et al.* (1977) for torsional vibrations.

Figure 5 shows a graph of S_s for the model *LYR* 4. The case when $n=1$ is given as an example because it is expected for small n that the modes are well decoupled into the *PKP*-type and *ScS*-type respectively even at low radial modes. This decoupling is proved from close resemblance between our curve and that for the toroidal modes (Fig. 6 of LAPWOOD and SATO, 1977). Almost straight dashed-lines link those points with recurrence period 10 in i. Detailed discussion on such patterns has been made by LAPWOOD and SATO (1977, 1978).

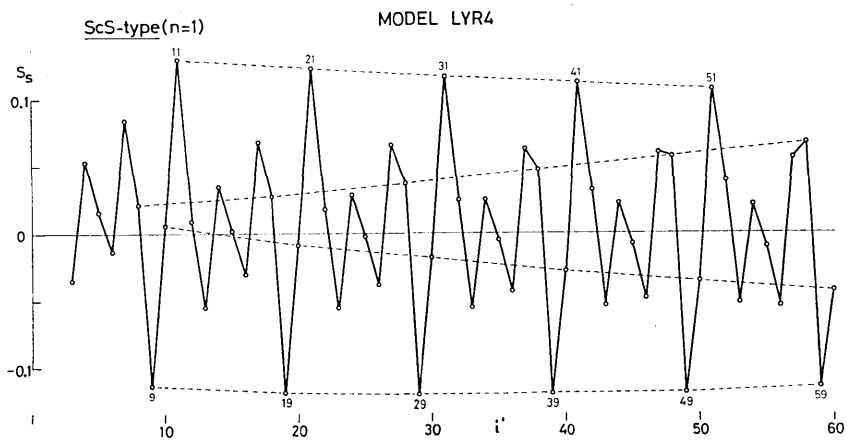

Fig. 5. Graph of S_s against i' for the model *LYR* 4. Computation is made for the angular order $n=1$. Dashed curves show the smoothly varying property of S_s at every 10 steps in i'.

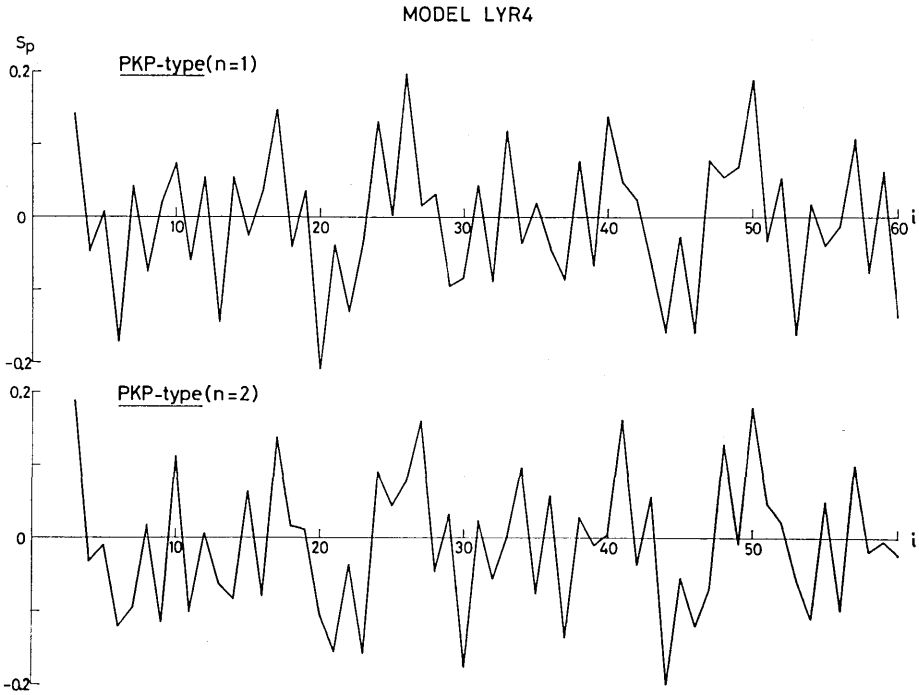

Fig. 6. Graphs of S_p against i for the model *LYR* 4. Computation is made for the angular order $n=1$ and 2.

After removing the eigenfrequencies of the *ScS*-type modes from the original composite solutions of Eq. (2.29), we can get graphs for the *PKP*-type modes (Fig. 6). These curves show more intricate patterns when compared with the previous examples. The approximate formula (4.6) suggests that these patterns consist of three sinusoidal curves with different amplitudes and periods specified by the constants $-R_1^P/\pi \simeq 0.09$, $-R_2^P/\pi \simeq 0.08$, $-R_3^P/\pi \simeq 0.05$, $t_p/t_1 \simeq 1.7$, $t_p/(t_3+t_4) \simeq 7.9$, $t_p/t_4 \simeq 11.9$, which we get from the elastic constants in Fig. 2. It is however very difficult to recognize any systematic variations in their patterns, even though close observation surely reveals them. This complication is mainly due to the large magnitudes of the discontinuities in the model, which are characteristic of averaged Earth models consisting of a small number of homogeneous layers. The patterns of S_p and S_s for such models will be widely different from those expected for the actual Earth. Hence, from the practical point of view, investigation has to be made for more realistic Earth models.

Here we introduce two models called *DSN* and *CNT* respectively (see Fig. 7). The crust/mantle structure of the model *DSN* is designed in accordance with Model 1066B presented by GILBERT and DZIEWONSKI (1975), which is characterized by two discontinuities in the upper

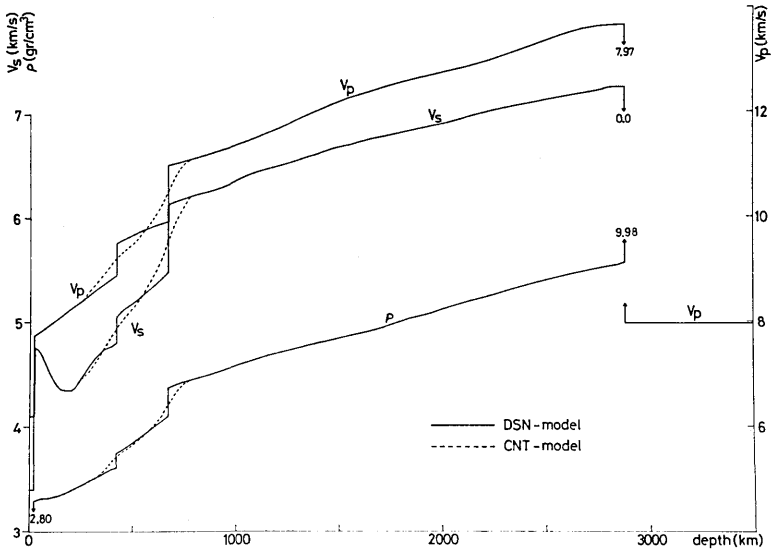

Fig. 7. Density, *P*- and *S*-wave velocity structures for two Earth models, *DSN* and *CNT*, which have discontinuous and continuous structures in the upper mantle respectively. The core is assumed to be homogeneous and liquid.

mantle. The model *CNT* has, on the other hand, a continuously varying structure through the whole space of the mantle, similar to Model 1066A of the above authors. A homogeneous liquid core is assumed for both models to emphasize the effect of difference in the upper-mantle structures on S_p- and S_s-patterns and to ensure high accuracy in numerical computation.

We have computed eigenfrequencies for the case $n=1$ with the use of Eq. (2.29), substituting 91 uniform layers for the whole mantle. Deviation of the frequencies from the zero order approximations, Eq. (4.2), is not very large in the present case as is expected for realistic models, and we can sort out the *PKP*-type and *ScS*-type modes with comparative ease by virtue of the relations (4.2) and (4.3).

In Fig. 8 (upper two graphs), S_p and S_s for the two models obtained in terms of Eq. (4.1) are plotted against i and i' respectively. For reference, the period of free oscillations is written in abscissa. It is found that their patterns are relatively simple compared with those for the previous averaged-Earth-models. There is a notable difference between solid curves (model *DSN*) and dashed curves (model *CNT*), resulting from the difference in the upper-mantle structure (with or without discontinuities). Then, existence of the discontinuities gives rise to large vibrations in their patterns. Good coincidence of the solid

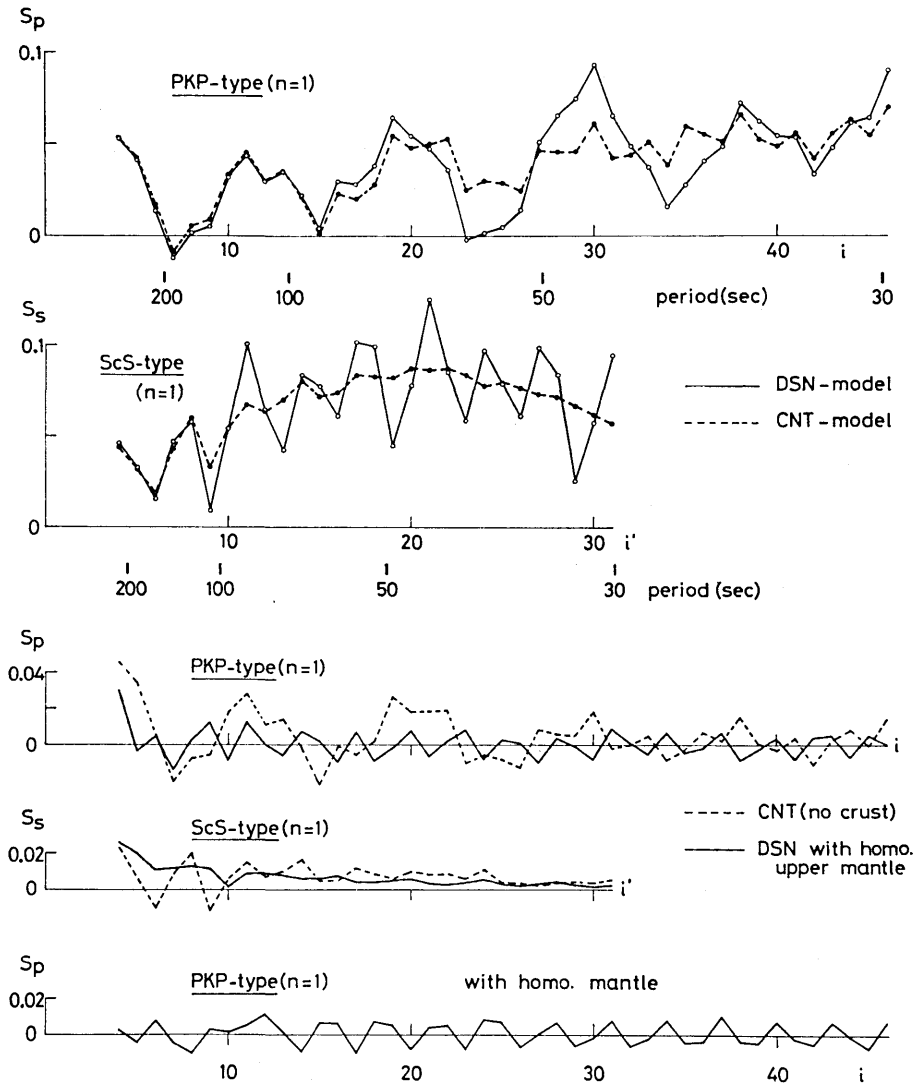

Fig. 8. Graphs of S_p against i (top) and S_s against i' (second) for the model *DSN* (solid curves) and *CNT* (dashed curves). For reference, the period of free oscillations is given in units of second in abscissa. The third and fourth graphs show S_p- and S_s-curves respectively for partially modified models, *CNT* without a crust (dashed curves) and *DSN* with a uniform upper mantle (solid curves). The bottom graph shows a S_p-curve for the model with a uniform mantle and core which keeps the same scale of discontinuity at the interface as that of the model *DSN* or *CNT*. All the computations are made for the angular order $n=1$.

and dashed curves at small i and i' is attributable to the situation that the whole upper mantle, where elastic parameters vary sharply

with depth in the small range of radial distance ($\lesssim$700km) compared with the radius of the Earth, acts as a discontinuity common in both models on the long-period free oscillations. This will be discussed later. Roughly speaking, the amplitudes and periods of the solid curves coincide with those estimated by Eq. (4.7) by applying it formally to the model *DSN* (putting $M=5$), because we get, for 671 km discontinuity, $-R_2^P/\pi \simeq 0.026$, $t_p/(t_3+t_4+t_5) \simeq 9.0$, $-R_2^S/\pi \simeq 0.028$, $t_s/(t_3'+t_4'+t_5') \simeq 3.3$ and for 420 km discontinuity, $-R_3^P/\pi \simeq 0.017$, $t_p/(t_4+t_5) \simeq 14$, $-R_3^S/\pi \simeq 0.014$, $t_s/(t_4'+t_5') \simeq 5.0$.

In the model *CNT* there still remain two discontinuities, the crust-mantle and mantle-core boundaries. From the previous discussion on the simple models, it can be inferred that the crust-mantle boundary gives rise to long-period oscillations, while the mantle-core boundary does short-period fluctuations. We can readily recognize large trends in the variations in the dashed curves of the upper two graphs. Their amplitudes and periods are approximately coincident with those estimated from Eq. (4.5) since we get, for the Moho discontinuity, $-R_2^P/\pi \simeq 0.06$, $t_p/t_3 \simeq 200$, and $-R_2^S/\pi \simeq 0.08$, $t_s/t_3' \simeq 80$.

Dashed curves of the third and fourth graphs are obtained for a model constructed by removing the Moho discontinuity from the model *CNT* (the crust being replaced by a uniform layer of which material is the same as that of the uppermost part of the mantle). Then, the large trends are clearly eliminated from both curves of the *PKP*-type and *ScS*-type. There still remain the oscillations with periods 7~8 in i in the S_p-curve, superimposed on the short-period fluctuations, and periods 3~4 in i' in the S_s-curve, both being conspicuous at the fore part of each curve. We call those components *middle-period oscillations*. There is no doubt that the short-period fluctuations are the "solo-tone effect" caused by the existence of the mantle-core boundary, the only explicit discontinuity in the present model. In fact, we cannot observe the corresponding fluctuations in the S_s-curve since it does not act as an internal boundary for the *ScS*-type modes.

The other discontinuity that we can imagine as the origin of the *middle-period oscillations* is the upper mantle itself, where the elastic parameters change continuously but very steeply. This speculation is proved to be true through the numerical computation for a model with a uniform upper-mantle. The model is designed in such a way that it has a uniform structure at depth less than 671 km and it links to the model *DSN* at depth 671 km without a first order discontinuity in its elastic parameters. Then, we get solid curves in the third and fourth graphs of Fig. 8. It shows that the *middle-period oscillations* are clearly eliminated from these curves by this modification. Here, it is

interesting to try to estimate the amplitudes of these *middle-period oscillations* in a similar manner as attempted above for other discontinuities. We can regard the whole upper-mantle as one *discontinuity* since only long-period free oscillations are concerned with this phenomenon. Then, assuming that the scale of the *discontinuity* is prescribed by maximum and minimum values of the elastic parameters in this region, we get, from Eq. (3.13), $-R^P/\pi \simeq 0.1$ and $-R^S/\pi \simeq 0.1$ for this *discontinuity* (put $\rho_i \sim 4.4$, $\alpha_i \sim 11$, $\beta_i \sim 6.2$, $\rho_{i+1} \sim 3.3$, $\alpha_{i+1} \sim 7.8$ and $\beta_{i+1} \sim 4.4$). These amplitudes are three to five times as large as those observed in the graphs. Hence, we can say that the effect of this *discontinuity* is in fact much reduced by its smoothly varying character. This tendency increases as period of free oscillations decreases, which is physically reasonable. Now, it is concluded that the solotone phenomenon is caused not only by an actual discontinuity but also by a continuously but steeply varying structure in the medium. In the latter case, its *pseudo solotone-effect* will depend on rate of change in structure with depth and wavelength of free oscillation.

The remaining short-period fluctuations in the *PKP*-type modes (solid curve in the third graph) still appear in the curve for a model with a uniform mantle and a liquid core (bottom graph) where the scale of discontinuity at the mantle-core boundary is retained as it is in the model *DSN*. These amplitudes and periods agree with those estimated from Eq. (4.4) since we get $-R_1^P/\pi \simeq 0.007$, $t_p/t_2 \simeq 3.1$ for this discontinuity.

Thus, the whole oscillatory features observed in the S_p- and S_s-curves are explainable in terms of an additive effect of individual "solotone effect" caused by the discontinuities explicit and implicit in the Earth. Then, the approximate formulas obtained for the layered models are, on the whole, valid for realistic models as well.

In general, S_p-curves have more complicated appearance than S_s-curves because all the discontinuities associated with the core affect the *PKIKP*-type modes (taking the inner core into account) but not the $(ScS)_V$-type modes (and $(ScS)_H$-type modes of the torsional oscillations as well). In this sense, the latter modes are more sensitive to differences in the mantle structure than the former modes. However there seems to be few observations of the $(ScS)_V$- and $(ScS)_H$-type modes. GILBERT and DZIEWONSKI (1975) have identified a lot of higher spheroidal and toroidal modes besides fundamental modes and compiled them together with other authors' data. Their table include, for example, relatively high order of the spheroidal modes with $n=1$ such as ${}_{26}S_1$, ${}_{29}S_1$, ${}_{32}S_1$ and ${}_{34}S_1$ in their notation. Estimating S_p and S_s for these modes from their data, we find that the values of S_p are dis-

tributed in the range of small amplitude while those of S_s deviate from the expected range. In the result, we can identify the above modes as the *PKIKP*-type with the radial mode numbers $i=11$, 12, 13 and 14 respectively in our notation, and thus high $(ScS)_V$-type modes seem to be missing from the observations. Figure 8 suggests that those modes with $i \leq 14$ are unfortunately insensitive to the existence of the discontinuities in the upper mantle, and a little higher *PKIKP*-type modes and the missing $(ScS)_V$-type modes (or the corresponding $(ScS)_H$-type modes) are required for confirming their existence in terms of the solotone phenomenon.

5. Summary

The matrix method is employed successfully for formulating the frequency equation of the spheroidal oscillations of the multi-layered Earth and for computing the eigenfrequencies of relatively high radial modes with small angular order numbers.

The method is also applied to demonstrating the decoupling of the equation at high frequencies and to deriving its explicit forms for the simple Earth models.

The solutions of the asymptotic frequency equations to the first order approximations well illustrate the effect of discontinuities in the Earth on the distribution of decoupled eigenfrequencies. It is that the amplitude and period of the "solotone effect" caused by an internal discontinuity depend on its scale and depth respectively and the effect is additive for two or more discontinuities.

The numerical experiments for the Earth with realistic mantle structures further reveal that a continuously but sharply varying structure in the medium causes the *pseudo solotone-effect* for the lower part of eigenfrequencies.

From a viewpoint of mode-ray duality, the normal modes that this paper is concerned with are closely connected with body waves which travel radially in the Earth. Then, P and S waves are decoupled from each other, and we have independent frequency equations corresponding to respective body waves. In the case when P and S waves are coupled, that is, the waves travel obliquely in the Earth, ray geometries become complicated and we get different forms of asymptotic frequency equations corresponding to different ray geometries. Investigation on this case will be made in the succeeding papers in terms of both mode theory and ray theory (ODAKA, 1980a, b).

Acknowledgement

The author wishes to express sincere thanks to Professor Tatsuo Usami, Earthquake Research Institute, the University of Tokyo, for making valuable suggestions in improving the manuscript and for encouragement throughout this study. The numerical computation was carried out on HITAC 8800/8700 system at the Computer Center, the University of Tokyo (Subject No. 1136013001).

References

ANDERSSEN, R. S., The effect of discontinuities in density and shear velocity on the asymptotic overtone structure of torsional eigenfrequencies of the Earth, *Geophys. J. R. Astron. Soc.*, **50**, 303-309, 1977.

ANDERSSEN, R. S. and J. R. CLEARY, Asymptotic structure in torsional free oscillations of the Earth—I. Overtone structure, *Geophys. J. R. Astron. Soc.*, **39**, 241-268, 1974.

ANDERSSEN, R. S., J. R. CLEARY, and A. M. DZIEWONSKI, Asymptotic structure in eigenfrequencies of spheroidal normal modes of the Earth, *Geophys. J. R. Astron. Soc.*, **43**, 1001-1005, 1975.

BEN-MENAHEM, A., Mode-ray duality, *Bull. Seismol. Soc. Am.*, **54**, 1315-1321, 1964a.

BEN-MENAHEM, A., Spectral response of an elastic sphere to dipolar point source, *Bull. Seismol. Soc. Am.*, **54**, 1323-1340, 1964b.

BHATTACHARYA, S. N., Extension of the Thomson-Haskell method to non-homogeneous spherical layers, *Geophys. J. R. Astron. Soc.*, **47**, 411-444, 1976.

DZIEWONSKI, A. M. and F. GILBERT, Observations of normal modes from 84 recordings of the Alaskan earthquake of 1964 March 28, *Geophys. J. R. Astron. Soc.*, **27**, 393-446, 1972.

GILBERT, F., Some asymptotic properties of the normal modes of the Earth, *Geophys. J. R. Astron. Soc.*, **43**, 1007-1011, 1975.

GILBERT, F. and A. M. DZIEWONSKI, An application of normal mode theory to the retrieval of structural parameters and source mechanisms from seismic spectra, *Phil. Trans. R. Soc., A*, **278**, 187-269, 1975.

GILBERT, F. and G. J. F. MACDONALD, Free oscillations of the Earth I. Toroidal oscillations, *J. Geophys. Res.*, **65**, 675-693, 1960.

LAPWOOD, E. R., The effect of discontinuities in density and rigidity on torsional eigenfrequencies of the Earth, *Geophys. J. R. Astron. Soc.*, **40**, 453-464, 1975.

LAPWOOD, E. R. and R. SATO, The asymptotic distribution of torsional eigenfrequencies of a spherical shell. III, *J. Phys. Earth*, **25**, 361-376, 1977.

LAPWOOD, E. R. and R. SATO, The pattern of eigenfrequencies of overtones of torsional oscillations of a layered spherical shell, *J. Comput. Phys.*, **29**, 412-420, 1978.

MCNABB, A., R. S. ANDERSSEN, and E. R. LAPWOOD, Asymptotic behavior of the eigenvalues of a Sturm-Liouville system with discontinuous coefficients, *J. Math. Anal. Appl.* **54**, 741-751, 1976.

ODAKA, T., Derivation of asymptotic frequency equations in terms of ray and normal mode theory and some related problems: Radial and spheroidal oscillations of an elastic sphere, *J. Phys. Earth*, **26**. 105-121, 1978.

ODAKA, T., Asymptotic frequency equations for spheroidal oscillations of a spherical Earth with a uniform mantle and core—Modes of finite phase velocity—, *Bull. Earthq. Res. Inst.*, **55**, 1980a (in press).

ODAKA, T., Ray-theoretical approach to frequency equations of spheroidal oscillations of a spherical Earth with a uniform or non-uniform mantle and core, 1980b (in preparation).

OKAL, E. A., A physical classification of the Earth's spheroidal modes, *J. Phys. Earth*, **26**, 75-103, 1978.

PHINNEY, R. A. and S. S. ALEXANDER, *P* wave diffraction theory and the structure of the core-mantle boundary, *J. Geophys. Res.*, **71**, 5959-5975, 1966.

SATO, R. and E. R. LAPWOOD, The asymptotic distribution of torsional eigenfrequencies of a spherical shell. I, *J. Phys. Earth*, **25**, 257-282, 1977a.

SATO, R. and E. R. LAPWOOD, The asymptotic distribution of torsional eigenfrequencies of a spherical shell. II, *J. Phys. Earth*, **25**, 345-360, 1977b.

SEZAWA, K., *Shindo-gaku*, Iwanami-shoten, 1932 (in Japanese).

USAMI, T., T. ODAKA, and Y. SATÔ, Theoretical seismograms and earthquake mechanism. Part I. Basic principles, Part II. Effect of time function on surface waves, *Bull. Earthq. Res. Inst.*, **48**, 533-579, 1970.

WANG, C., J. F. GETTRUST, and J. R. CLEARY, Asymptotic overtone structure in eigenfrequencies of torsional normal modes of the Earth: A model study, *Geophys. J. R. Astron. Soc.*, **50**, 289-302, 1977.

WATSON, G. N., *A treatise on the theory of Bessel function*, Cambridge Univ. Press (2nd ed.), p. 804, 1952.

---

1. 多層構造弾性球の伸び縮み振動における高次モードの固有振動数の挙動

— 高位相速度のモード —

地震研究所　小　高　俊　一

地殻・マントル・外核（流体）・内核（固体）を有する弾性球の，伸び縮み振動の特性方程式を，matrix 法 (Thomson-Haskell 法) で求めた．その結果を用い，方程式の漸近形（余緯度方向の次数を固定しておいて短周期近似を行う）の考察を行った．それによると，特性方程式は三種類の実体波，*PKIKP*, $(ScS)_V$, *J* に対応し，三つの独立な方程式に分離する．これは波線理論的には，*P* 波，*S* 波が半径方向（表面に垂直）に伝播し，$P \leftrightarrow S$ の波の転換が生じず，*PKIKP*, $(ScS)_V$, *J*（内核内の *S* 波）がそれぞれ独立に振舞うことに対応している．

次に，単純なモデル（均質な流体核と 1～3 層から成るマントルを有する球）に対し，漸近的特性方程式の具体的な形を得た．この場合，*PKP* と $(ScS)_V$ に対応する独立な二つの方程式が得られる．更にその第零次，第一次近似解を得た．その表現式より，媒質内の不連続の大きさ，深さが固有振動数の分布のパターンに与える影響を知ることが出来る．近似解の有効性を調べるために，単純なモデルに対し数値計算を行った．

現実的なマントル構造を有する二つのモデル（核は均質な流体とする）に対して，不連続面の影響を数値実験的に調べた．一方のモデルは上部マントルにいわゆる 400 km と 600 km の不連続面を有し，他方は連続的に変化する構造を有する．前者に対する固有振動数の分布のパターンは振動的で，いゆわる solotone effect が見られ，後者に対するパターンは比較的滑らかで，両者の違いは顕著である．他に，モホ不連続面，マントル-核の境界の影響による solotone effect が付加される．ここで注目すべきことは，上部マントルの構造が連続的に変化する場合でも，長周期の振動に対しては solotone effect に類似したパターンが現われることである．これは，構造が深さと共に急激に変化しているため，実際の不連続面と同等の効果を及ぼすことによると考えられる．